Chinese Chemical Letters 33 (2022) 3869–3872

Contents lists available at ScienceDirect

Chinese Chemical Letters

journal homepage: www.elsevier.com/locate/cclet

Two-dimensional MOF Cu-BDC nanosheets/ILs@silica core-shell composites as mixed-mode stationary phase for high performance liquid chromatography

Tiantian Si[a,c], Xiaofeng Lu[a], Haixia Zhang[b], Shuai Wang[a], Xiaojing Liang[a,*], Yong Guo[a,*]

[a] CAS Key Laboratory of Chemistry of Northwestern Plant Resources and Key Laboratory for Natural Medicine of Gansu Province, Lanzhou Institute of Chemical Physics, Chinese Academy of Sciences, Lanzhou 730000, China
[b] State Key Laboratory of Applied Organic Chemistry and College of Chemistry and Chemical Engineering, Lanzhou University, Lanzhou 730000, China
[c] University of Chinese Academy of Sciences, Beijing 100049, China

ARTICLE INFO

Article history:
Received 21 July 2021
Revised 8 September 2021
Accepted 17 October 2021
Available online 23 October 2021

Keywords:
2D MOF composites
Chromatographic separation
Liquid chromatography
Mixed-mode
Stationary phase

ABSTRACT

Here, silica microspheres were decorated with two-dimensional metal–organic frameworks (2D MOFs) nanosheets and ionic liquids, and evaluated as the mixed-mode stationary phase for chromatographic separation. The ionic liquids were used to assist the synthesis of 2D MOFs nanosheets, and also acted as adhesives among the nanosheets and silica. In contrast with the 2D MOFs-based column without ionic liquids and commercial columns, the prepared column exhibited enhanced chromatographic separation performance for partially hydrophilic compounds such as alkaloids, sulfonamides and antibiotics, etc. In addition to excellent chromatographic repeatability and stability, it has also been verified that the composites could be easily and repeatedly prepared. The relative standard deviation of the retention time of the same type of analyte between the three batches of materials was ranging from 0.21% to 1.7%. In short, these results indicated that the synthesized composites were promising separation material for liquid chromatography, which made it possible to broaden the application of 2D MOFs in the field of chromatography.

Metal–organic frameworks (MOFs) with well-defined architecture and high specific surface area have emerged as promising candidates to address the challenge of catalysis [1–3], sensing and electrochemistry [4,5], drug delivery and imaging [6–8], gas storage and gas separation [9–11] in the past few decades. In virtue of their structural and functional diversity, MOFs have been demonstrated as prominent materials in chromatographic separation-related applications [12,13]. Compared with other media-modified silica-based chromatographic stationary phases, the unique structure of MOFs makes them have molecular sieving effect, allowing easy separation of compounds with similar structures. Hereby, a variety of MOFs-based core-shell composites have been developed gradually, and superseded the original MOFs particles as stationary phases in the field of chromatographic stationary phases [14–16]. The three-dimensional (3D) MOFs were widely exploited and developed in the MOFs-based composite materials mentioned above. Nevertheless, the biggest problem of 3D MOFs-based stationary phase is their relatively low mass transfer rate, which limits their separation and analysis efficiency.

Two-dimensional (2D) MOFs nanosheets possess the characteristics of both 3D MOFs and 2D nanomaterials. The merits containing structural simplicity, abundant accessible active sites and highly ordered pore arrays make them a new competitive type of 2D nanomaterials [17–19]. Recent studies also revealed that 2D MOFs with short pathways for mass transport and bare metallic ions create an opportunity for chromatographic separation and analysis [18]. 2D MOF nanosheets can be prepared by a variety of methods. They have evolved from the early direct ultrasonic dissection and direct synthesis to the current adjuvant ultrasonic dissection and modulation synthesis [4,19,20]. In the previous study, we have reported that 2D MOF-FDM-23 nanosheets were obtained directly by ultrasound in an aqueous solution and were modified on the surface of silica as hydrophilic stationary phase [21]. Compared with the previous 3D MOFs-based stationary phases, the hydrophilic separation performance was enhanced, but it was also restricted to be used for hydrophilic separation.

Apart from the above direct ultrasound strategies, incorporating assistant materials can be an effective route to improve MOFs/silica

* Corresponding authors.
E-mail addresses: xjliang@licp.cas.cn (X. Liang), guoyong@licp.cas.cn (Y. Guo).

https://doi.org/10.1016/j.cclet.2021.10.048
1001-8417/

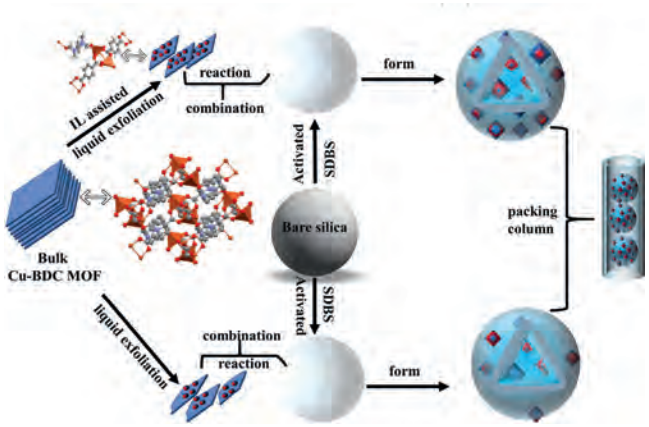

Fig. 1. Schematic diagram of the preparation route of the 2D Cu-BDC/IL@silica composites.

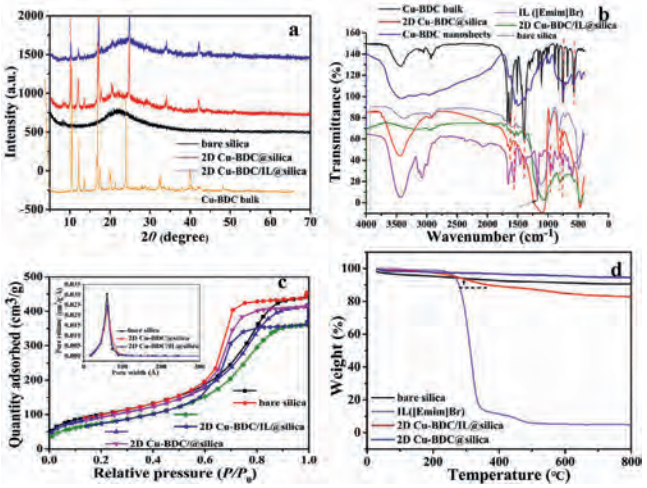

Fig. 2. (a) The PXRD results of bare silica, Cu-BDC bulk, 2D Cu-BDC/IL@silica, and 2D Cu-BDC@silica. (b) FTIR spectra results of Cu-BDC bulk, 2D Cu-BDC nanosheets, IL ([Emim]Br), 2D Cu-BDC/IL@silica, and 2D Cu-BDC@silica. (c) The N_2 adsorption-desorption isotherms and the pore size distribution of bare silica, 2D Cu-BDC/IL@silica, and 2D Cu-BDC@silica. (d) The TGA of bare silica, IL ([Emim]Br), 2D Cu-BDC/IL@silica, and 2D Cu-BDC@silica.

interface and composite performance [22]. Considering that the crystal structure of Cu-BDC belongs to monoclinic, the intrinsic structure anisotropy is possible for 2D growth of the MOFs. The obvious lamellar stacked structure of Cu-BDC bulk MOF makes it easy to peeled off under the action of ultrasound. Moreover, it also has excellent water stability. Ionic liquids (ILs), as the selective adsorption and extremely low volatility materials, can be good candidates because of their attractive physicochemical properties [23–25]. Herein, the imidazole-based ILs ([Emim]Br) with low viscosity and high hydrophilicity was selected to assist the synthesis of 2D Cu-BDC nanosheets and can also be used as an adhesive between 2D Cu-BDC nanosheets and silica. The composites were further used as mixed-mode stationary phase to separate a variety of hydrophilic and hydrophobic compounds including alkaloids, sulfonamides, antibiotics and anilines, etc. Compared with the 2D MOF Cu-BDC@silica column, it exhibited enhanced chromatographic separation performance and superior chromatographic stability.

Cu-BDC bulk material was prepared according to a previously reported method [17]. The details of the synthesis including the pretreatment of the bare silica, Cu-BDC nanosheets, 2D Cu-BDC/IL@silica composites and 2D Cu-BDC@silica composites can be found in the supporting information (ESM). As shown in Fig. 1, it illustrated the protocol for synthesizing the 2D MOF Cu-BDC nanoflakes and the nanoflakes/IL-assembled core-shell superstructure.

The morphologies of the samples were studied by field emission scanning electron microscopy (SEM) transmission electron microscopy (TEM). The TEM figures of bare silica and 2D Cu-BDC nanosheets were shown in Figs. S1a and b (Supporting information), respectively. As shown in Fig. S1c (Supporting information), the surface of silica was modified by original 2D MOF Cu-BDC nanoflakes. Meanwhile, 2D MOF Cu-BDC nanoflakes with ILs were co-modified on the surface of silica as shown in Fig. S1d (Supporting information). By comparison, it can be found that the surface of the silica co-modified by ILs and 2D Cu-BDC nanosheets was more uniform, and solidified on the surface of the silica. Similarly, the uniform distribution of C and N elements can also be found in the energy dispersive X-ray spectroscopy (EDS) mapping in Figs. S1e–h (Supporting information). As shown in Fig. S2 (Supporting information), it showed the images of Cu-BDC bulk, 2D Cu-BDC nanosheets prepared in different ways, and bare silica microspheres and modified silica microspheres. It also showed intuitively that 2D Cu-BDC nanosheets with different morphologies can be obtained by processing the layered Cu-BDC bulk with different processing methods, and the surface of the silica microspheres has been modified in different ways.

The X-ray diffraction (XRD) patterns of the Cu-BDC bulk, bare silica, 2D Cu-BDC@silica and 2D Cu-BDC/IL@silica composites were shown in Fig. 2a. The main peaks of the as-prepared 2D Cu-BDC@silica and 2D Cu-BDC/IL@silica composites were identical to that of the Cu-BDC bulk powder pattern indicating no damage to the crystal structure of Cu-BDC MOF during the preparation step. Meanwhile, it can be observed these XRD patterns of 2D Cu-BDC@silica and 2D Cu-BDC/IL@silica composites showed slightly different relative intensity, which can be attributed to ILs filling the pores. Fourier-transform infrared spectroscopy (FTIR) spectra (Fig. 2b) of both 2D Cu-BDC@silica and 2D Cu-BDC/IL@silica revealed bands at 1000−1600 cm^{-1}, indicating the presence of benzene rings of H_2BDC ligand. The bands at 1665.7, 1624.3 and 1439.6 cm^{-1} belonging to the antisymmetric and symmetric stretch modes of the −COO− groups were characterized. The C−O−Cu stretching exhibited the characteristic band at 1106 cm^{-1}, which can be found in the Cu-BDC bulk, 2D Cu-BDC@silica and 2D Cu-BDC/IL@silica composites. The bands at 700–1500 cm^{-1} were representative of the vibration of the imidazole ring. The bands at 1624, 866 and 752 cm^{-1} could be clearly found in the ILs ([Emim]Br) and 2D Cu-BDC/IL@silica composites, while the 2D Cu-BDC@silica did not.

Compared with bare silica, the surface area of 2D Cu-BDC@silica and 2D Cu-BDC/IL@silica has gradually decreased from 365.7 m^2/g to 339.8 m^2/g or 277.2 m^2/g. (Fig. 2c and Table S1 in Supporting information) As displayed in Fig. 2c, like the surface areas, the pore volumes have also decreased from 0.71 cm^3/g (bare silica) to 0.56 cm^3/g (2D Cu-BDC/IL@silica). It should be noted that the original surface and pore diameter of bare silica were changed by 2D Cu-BDC nanosheets and ILs. The thermal stability of these composites was studied by using thermogravimetric analysis (TGA). As shown in Fig. 2d, the characteristic temperature of thermal decomposition of ILs ([Emim]Br) was 350 °C, at which time the weight loss rate was the largest. Therefore, the calcination temperature in the process of preparing the 2D Cu-BDC/IL@silica composites were chosen to be 300 °C, so that part of the ILs can be carbonized and another part of the ILs can be retained at the same time. It was also confirmed by the comparison of chromatographic separation

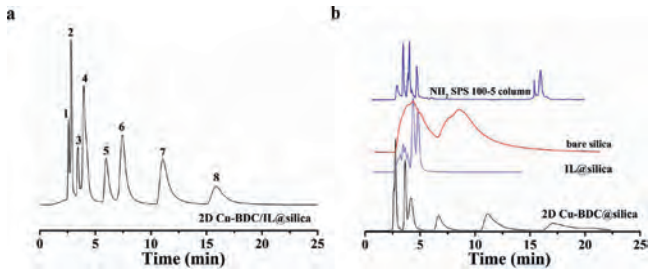

Fig. 3. Chromatograms for the separation of eight alkaloids on 2D Cu-BDC/IL@silica, NH_2 SPS 100–5, bare silica, Il@silica and 2D Cu-BDC@silica columns. sanguinarine (1), caffeine (2), theophylline 7 (3), theobromine (4), berberine (5), palmatine chloride (6), jatrorrhizine (7) and coptisine (8); mobile phase: (a) 80% acetonitrile, 20% 0.2% triethylamine aqueous solution, flow rate = 0.8 mL/min, T = 25 °C, UV detection: 254 nm; (b) 0–2 min 92% acetonitrile, 2–2.1 min 85% acetonitrile, the other phase is 0.2% triethylamine aqueous solution. The other conditions are consistent with 2D Cu-BDC/IL@silica column.

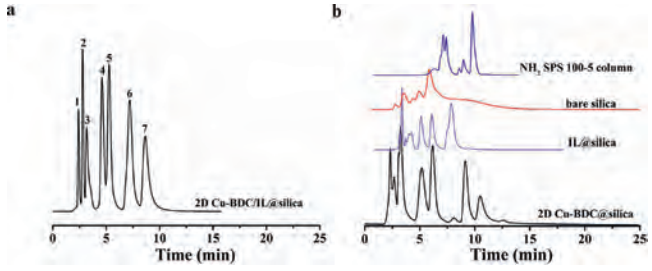

Fig. 4. Chromatograms for the separation of seven sulfonamides on 2D Cu-BDC/IL@silica column, NH_2 SPS 100–5, bare silica, Il@silica and 2D Cu-BDC@silica columns. sulfamethazine (1), sulfisoxazole (2), sulfadiazine (3), sulfaguanidine (4), sulfasalazine (5) sulfisoxazole (6), sulfamethoxazole (7); mobile phase: (a) 80% acetonitrile 20% 100 mmol/L ammonium acetate solution, flow rate = 0.8 mL/min, T = 25 °C, UV detection: 254 nm; (b) 0–5 min 85% acetonitrile, 5–6 min 75% acetonitrile, another phase is 100 mmol/L ammonium acetate solution. The other conditions are consistent with 2D Cu-BDC/IL@silica column.

performance. The elemental analysis data of bare silica, 2D Cu-BDC@silica and 2D Cu-BDC/IL@silica were listed in Table S2 (Supporting information). The gradually increased carbon content also indicated that it was feasible to choose 300 °C. The results of X-ray photoelectron spectroscopy (XPS) and EDS energy spectrum further confirmed the successful synthesis of 2D Cu-BDC/IL@silica with the increase of C, H, O and N elements as shown in the Figs. S3–S5 and Table S3 (Supporting information).

To investigate the hydrophilic separation performance of the 2D Cu-BDC/IL@silica column and the respective roles of ILs or 2D Cu-BDC nanosheets, eight alkaloids were separated on the 2D Cu-BDC/IL@silica, bare silica, NH_2 SPS 100–5, IL@silica and 2D Cu-BDC@silica columns. As shown in Fig. 3, the separation performance of alkaloids on the original IL@silica and the 2D Cu-BDC@silica columns were far inferior to that of the 2D Cu-BDC/IL@silica column. It seemed that ILs and 2D Cu-BDC nanosheets were complementary and synergistic in terms of separation capacity. It also proved that the addition of ILs was beneficial to hydrophilic separation.

As shown in Fig. 4, seven sulfonamides were separated on the 2D Cu-BDC/IL@silica, IL@silica, commercial NH_2 SPS 100–5 and bare silica columns. A satisfied result of separation was obtained on the 2D Cu-BDC/IL@silica column, however, this result was not obtained on commercial NH_2 SPS 100–5 and bare silica columns. Meanwhile, the poor separation of broadening peaks and inferior column efficiency was given on the IL@silica and bare silica columns. As shown in Fig. S6 (Supporting information), six nucleosides and nucleobases were completely separated on the 2D Cu-BDC/IL@silica and commercial NH_2 SPS 100–5 column. However, the separation performance of antibiotics on the commercial NH_2 SPS 100–5 column was worse than that of the 2D Cu-BDC/IL@silica column (Fig. S7 in Supporting information). In addition, the separation results of antibiotics on the 2D Cu-BDC/IL@silica column were not satisfactory. Because the structures of these types of antibiotics are very similar or complex, and they may have strong or similar interactions with functional groups and MOFs nanosheets, all of which make the separation resolution on these columns is bad. It also confirmed that the silica surface-modified 2D Cu-BDC nanosheets and ILs have better selectivity and superior chromatographic separation performance for antibiotics.

The chromatographic behaviors of the prepared stationary phase were also evaluated under reversed-phase conditions. A test mixture of benzoic acids was used to evaluate the hydrophobic selectivity of the 2D Cu-BDC/IL@silica column, and the separation chromatograms together with that on C18 column were shown in Fig. S8 (Supporting information). In addition, Fig. S9 (Supporting information) showed the separation of PAHs using a water–acetonitrile mixture (70:30, v/v) as a mobile phase. Similarly, the separation of six kinds of alkylbenzenes was also shown in Fig. S10 (Supporting information), and the peak sequence of them was the same as that of C18 column. However, their separation resolution is much lower than that of PAHs. It may be that the separation of alkylbenzenes on the 2D Cu-BDC/IL@silica column mainly relies on hydrophobic interactions, while PAHs also have π-π interactions in addition to hydrophobic interactions.

The hydrophilic interaction liquid chromatography (HILIC) retention mechanism of the 2D Cu-BDC/IL@silica column was evaluated by investigating the changes of retention time of hydrophilic solutes (including nucleosides and bases) with the content of water in mobile phase, and the results are expressed as trend curves of retention factors *versus* water volume fractions in Fig. S11a (Supporting information). It exhibited a decrease when the water volume fraction increases on the 2D Cu-BDC/IL@silica column, indicating typical HILIC retention behavior. It has been explained by an equation combining the distribution and adsorption model [26,27]. The retention factors for HILIC were generalized by Eq. 1:

$$\ln k = a + b\ln\varphi + c\varphi \quad (1)$$

In Eq. 1, k is the retention factor of the analytes; φ is the water fraction in the mobile phase; a, b, and c are all constants; It showed excellent fits ($R^2 = 0.9977$–0.9992) for nucleosides and bases at different eluent compositions ($\phi = 0.15$–0.35) in Fig. S11a and Table S4 (Supporting information). It proved that the retention mechanism of nucleosides and bases in the separation system was related to both adsorption and partitioning. It also certificated that the adsorption-desorption of MOFs also dominated the separation process. Therefore, in order to further explore and understand other retention behaviors, the effect of ACN content in mobile phase and pH was also investigated (Figs. S11 and S12 in Supporting information). As shown in Fig. S13 (Supporting information), PAHs and alkylbenzenes could not be separated on the 2D Cu-BDC@silica column. It also confirmed that partially carbonized ILs provided hydrophobic separation for the composites. The details of the discussions can be found in the ESM.

The repeatability and chemical stability are critical parameters for chromatographic stationary phases. It illustrated the reproducibility of the 2D Cu-BDC/IL@silica column by separation of sulfonamides with 10 continuous injections (Fig. S14a in Supporting information), and stability of the 2D Cu-BDC/IL@silica column was illustrated by against continuous aggressive high pH mobile phase (Fig. S14b in Supporting information)). As shown in Fig. S14b, the mixture of sulfonamides was injected by every 5 h for 20 h without recycling the mobile phase, which did not show any significant

Table 1
Standard addition and recovery of actual samples.

Samples	Analytes	Linear range (μg/L)	Calibration curve	Limits of detection (μg/L)	R^2	Recovery (%)
Milk	Cefotaxime sodium	0.5–250	$y = 1.3368x + 47.248$	0.1	0.9967	82.5–101.2
	Ceftizoxime	1–250	$y = 0.4434x + 33.885$	0.5	0.9902	79.6–102.4

drift in retention times. The RSDs of the retention times were listed in Table S4.

Long term used stability was also explored by continuous operation over 100 h with a mobile phase containing acetonitrile and 100 mmol/L ammonium acetate solutions. The difference of retention time and/or column efficiency of sulfonamides was shown by the RSD less than 0.92% (Fig. S15a and Table S5 in Supporting information). Furthermore, the reproducibility of batch-to-batch material preparation was investigated by the separation of six nucleosides and nucleobases on the three batches 2D Cu-BDC/IL@silica columns. As shown in Figs. S15 and S16 (Supporting information), there was no significant difference in separation performance between batches, and the RSDs of the retention times and/or column efficiency were listed in Table S6 (Supporting information). The column efficiencies of hydrophilic and hydrophobic compounds were investigated separately, which reached up to 8963.6 plates/m and 4811.2 plates/m in the Table S7 (Supporting information), respectively. In addition, a comprehensive comparison with similar works was shown in Table S8 (Supporting information). Compared with the previous work, the column efficiency was appropriately improved. Further work would be undertaken to reduce the particle size of silica microspheres and make MOFs with uniform particle size distribution.

The antibiotics were selected as targets and added to the actual samples of milk for testing. The specific details of the preparation were in the ESM. As depicted in Fig. S17 (Supporting information), it showed separation for the standards of antibiotics (a) and the spiked sample (b). In addition, the results of spiked recovery in actual samples were shown in Table 1. It was certain that the embedded endowed 2D Cu-BDC nanosheets and ILs the stationary phase with good hydrophilicity and huge application potential in actual samples.

The core shell composites were decorated with 2D Cu-BDC nanosheets and ILs, and prepared by ILs-assisted solvothermal synthesis. It has been introduced as a mixed-mode stationary phase for chromatography separation. Compared with the 2D Cu-BDC@silica, IL@silica and bare silica columns, the 2D Cu-BDC/IL@silica column exhibited enhanced selectivity and excellent stability. Compared with commercial columns, the 2D Cu-BDC/IL@silica stationary phase has low column efficiency for some compounds, but it still shows strong chromatographic separation development potential. In conclusion, the 2D Cu-BDC/IL@silica stationary phase possessed superior stability including pH stability and exhibited enhanced selectivity to a variety of hydrophilic and hydrophobic compounds.

Declaration of competing interest

The authors declare that they have no known competing financial interests or personal relationships that could have appeared to influence the work reported in this paper.

Acknowledgments

This work was supported by the National Natural Science Foundation of China (Nos. 21575149, 21575148) and the State Key Scientific Special Project (No. 2016ZX05011–003).

Supplementary materials

Supplementary material associated with this article can be found, in the online version, at doi:10.1016/j.cclet.2021.10.048.

References

[1] Y. Yang, X. Zhang, S. Kanchanakungwankul, et al., J. Am. Chem. Soc. 142 (2020) 21169–21177.
[2] Z. Jiang, X. Xu, Y. Ma, et al., Nature 586 (2020) 549–554.
[3] W. Yan, S. Li, T. Yang, et al., J. Am. Chem. Soc. 142 (2020) 16182–16187.
[4] H. Xia, J. Zhang, Z. Yang, et al., Nanomicro Lett. 9 (2017) 43.
[5] C. Qu, Y. Jiao, B. Zhao, et al., Nano Energy 26 (2016) 66–73.
[6] M. Chen, R. Dong, J. Zhang, et al., ACS Appl. Mater. Interfaces 13 (2021) 18554–18562.
[7] Y. Zhou, Z. Chen, D. Zhao, et al., Adv. Mater. 33 (2021) 2102044.
[8] S.S. Yang, Y.J. Chang, H. Zhang, et al., Anal. Chem. 90 (2018) 13796–13805.
[9] D. Alezi, Y. Belmabkhout, M. Suyetin, et al., J. Am. Chem. Soc. 137 (2015) 13308–13318.
[10] A. Ahmed, S. Seth, J. Purewal, et al., Nat. Commun. 10 (2019) 1568.
[11] M.H. Yu, B. Space, D. Franz, et al., J. Am. Chem. Soc. 141 (2019) 17703–17712.
[12] C.X. Yang, X.P. Yan, Anal. Chem. 83 (2011) 7144–7150.
[13] Y. Yu, N. Xu, J. Zhang, B. Wang, et al., ACS Appl. Mater. Interfaces 12 (2020) 16903–16911.
[14] R.D. Arrua, A. Peristyy, P.N. Nesterenko, Analyst 142 (2017) 517–524.
[15] S. Ehrling, C. Kutzscher, P. Freund, P. Müller, et al., Microporous Mesoporous Mater. 263 (2018) 268–274.
[16] Q. Qu, H. Xuan, K. Zhang, et al., J. Chromatogr. A 1505 (2017) 63–68.
[17] G. Zhan, L. Fan, F. Zhao, et al., Adv. Funct. Mater. 29 (2019) 1806720.
[18] Z.R. Tao, J.X. Wu, Y.J. Zhao, et al., Nat. Commun. 10 (2019) 2911.
[19] H. Jia, Y. Yao, J. Zhao, et al., J. Mater. Chem. A 6 (2018) 1188–1195.
[20] M. Wang, R. Dong, X. Feng, Chem. Soc. Rev. 50 (2021) 2764–2793.
[21] T. Si, X. Liang, X. Lu, et al., Talanta 222 (2021) 121603.
[22] R. Lin, L. Ge, H. Diao, V. Rudolph, et al., ACS Appl. Mater. Interfaces 8 (2016) 32041–32049.
[23] D. Jiang, J. Chen, M. Guan, et al., Talanta 233 (2021) 122513.
[24] H. Qiu, M. Takafuji, X. Liu, et al., J. Chromatogr. A 1217 (2010) 5190–5196.
[25] Q.Q. Wei, M.L. Qi, R.N. Fu, Chin. Chem. Lett. 20 (2009) 1111–1114.
[26] S. Zhang, F. Zhang, B. Yang, et al., Chin. Chem. Lett. 30 (2019) 470–472.
[27] Y. Guo, S. Gaiki, J. Chromatogr. A 1218 (2011) 5920–5938.